REVIEWED COMMENTARY
doi:10.26443/seismica.v5i1.2083

Commentary on 'A compilation of elastic anisotropy measurements from metamorphic rocks' by N.I. Christensen

Douglas R. Schmitt[1]

[1]Department of Earth, Atmospheric, and Planetary Sciences, Purdue University, West Lafayette, IN, USA

Overview My purpose in this commentary is to provide further context to Christensen (2026) in this issue of Seismica in order to fill some gaps so that readers better understand how the measurements are made, know what the analyses are based on, and know where the pitfalls in employing these results might lie. My experiences in reviewing and editing have revealed that many papers that focus on elastic or seismic anisotropy err as they are written often without understanding the basic principles. This problem is aggravated because some modern methods, such as Electron Backscatter Diffraction (EBSD), have made calculation of the anisotropy of metamorphic rocks readily accessible and production of figures perhaps too easy. I hope to both amplify and clarify the results archived in Christensen (2026) so they are not similarly misused and to provide readers with some tutorial background and more in-depth sources in order that they can avoid overinterpretation of anisotropy results more generally.

Production Editor:
Christie Rowe
Handling Editor:
Pathikrit Bhattacharya
Copy & Layout Editor:
Hannah F. Mark

Received:
October 20, 2025
Accepted:
December 18, 2025
Published:
February 9, 2026

1 Metamorphic Rock Symmetries

Symmetry is one important aspect mentioned in Christensen (2026) that is often overlooked elsewhere. Any discussion of anisotropy relies on the understanding of a given material's structural symmetry that is generally classified on the basis of symmetry operations which when applied leave the material's properties unchanged. Symmetry operations consist of various n-fold rotations, reflections in a plane, or their combinations. The details of such operations and descriptions of symmetry are beyond the scope here but are found in numerous classic texts on crystallography and mineralogy (e.g., Klein et al., 1993; Nye, 1985). The symmetries of mineral crystals fall within 7 crystal systems named in order of decreasing symmetry as cubic, hexagonal, trigonal, tetragonal, orthorhombic, monoclinic, and triclinic derived from 32-point groups. However, Brugger (1965) notes that wave propagation is centrosymmetric (i.e., velocities depend on direction but not sense of propagation) and hence an anisotropic material is categorized within 11 Laue groups that now further include isotropic.

Paterson and Weiss (1961), cited in Christensen (2026), extensively review these concepts in detail and discuss relationships to physical properties. They also provide a thorough analysis of metamorphic rock textural symmetries that they assert arise in a statistical sense from the orientation distributions of crystallographic axes, inequant grain shapes, lineations, bedding or foliation planes, fold axes, compositional layering, pores, and cracks (see their Table 5). Such orientational statistics are usually quantified via contouring in stereographic projections. For tectonites, they list the possible symmetries to be spherical (isotropic), axial (also referred to as transversely isotropic, radial, or hexagonal with this last designation used in Christensen (2026) and hereafter), orthorhombic, monoclinic, and triclinic that they support with illustrative stereographic projections of crystal orientations in various rocks. Paterson and Weiss (1961) make an important point that the overall bulk material symmetry cannot be greater than the 'subsymmetries' of the components. It may be also useful to note that the spherical fabric (which we would now more usually refer to as isotropic) is not a crystal system as are the less symmetric fabrics. One key point made in Christensen (2026) is that many metamorphic rocks may be characterized by hexagonal or orthorhombic symmetries as illustrated from sets of three orthogonal thin sections of metasediments from the Annabel Lake shear zone, Saskatchewan with hexagonal (Figure 1a) and orthorhombic (Figure 1b) symmetries. Readers are directed to Winterstein (1990) and Crampin (1984) for more detailed but clear discussions of elasticity and symmetry in the context of seismic anisotropy.

There is one practical problem that is difficult to overcome for experimentalists who work with anisotropic rocks. Unlike single crystals, the degree of symmetry and subsequent orientation of a sample within an XYZ co-ordinate system is often subjective. It is often challenging to assign the foliation plane or lineation direction exactly, and in some cases these visible features may not correlate with less obvious structural features such as lattice preferred orientations. Coring or machining of samples is with respect to the assigned co-ordinate system can also be challenging. This ambiguity of the material orientation will lead to some error in the analysis of anisotropy that as shown below assumes velocity measurements are made in prescribed directions with respect to the symmetry.

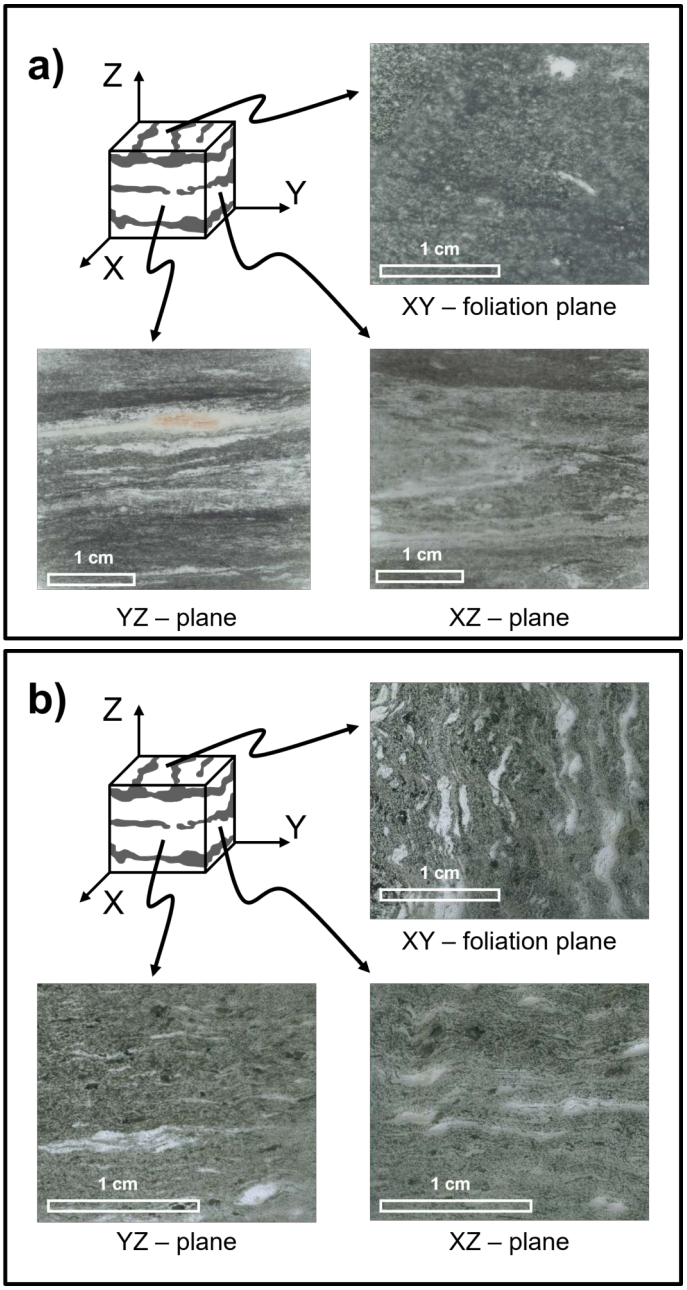

Figure 1 a) Orthogonal thin sections cut from deformed metavolcanics sample 93-1. Co-ordinate system is defined with respect to the visible fabric elements of foliation with principal axes X and Y defining the foliation plane. No lineated texture is seen in the X-Y plane indicating that the material has hexagonal symmetry as supported by the corresponding wave speed measurements. b) Orthogonal thin sections cut from deformed metavolcanic sample 93-7. Co-ordinate system defined with respect to the foliation plane (X-Y) and with the lineation within the XZ plane indicating orthorhombic symmetry. Wave speed measurements in the X, Y, and Z directions agree with these symmetries. Adapted from (Cholach et al., 2005) according to author use guidelines.

2 Relations Between Symmetry, Elasticity, Wave Speeds, and Polarizations

Knowing a material's symmetry is key to understanding its elastic properties. To add further context to Christensen (2026), it is worthwhile delving briefly into some of the underlying mathematical principles that the relationships that the manuscript relies on but does not explicitly include. This is done only superficially here to better link symmetry to the seismic properties and elasticity starting with the simpler Voigt reduced representation of Hooke's relationship between stress and strain:

$$\begin{bmatrix}\sigma_{11}\\ \sigma_{22}\\ \sigma_{33}\\ \sigma_{23}\\ \sigma_{31}\\ \sigma_{12}\end{bmatrix} = \begin{bmatrix}C_{11} & C_{12} & C_{13} & C_{14} & C_{15} & C_{16}\\ C_{21} & C_{22} & C_{23} & C_{24} & C_{25} & C_{26}\\ C_{31} & C_{32} & C_{33} & C_{34} & C_{35} & C_{36}\\ C_{41} & C_{42} & C_{43} & C_{44} & C_{45} & C_{46}\\ C_{51} & C_{52} & C_{53} & C_{54} & C_{55} & C_{56}\\ C_{61} & C_{62} & C_{63} & C_{64} & C_{65} & C_{66}\end{bmatrix} \begin{bmatrix}\epsilon_{11}\\ \epsilon_{22}\\ \epsilon_{33}\\ 2\epsilon_{23}\\ 2\epsilon_{31}\\ 2\epsilon_{12}\end{bmatrix} \tag{1}$$

where the σ_{ij} and ϵ_{ij} are the components of the stress and strain tensors, respectively, given in a convenient vector format and the C_{ij} are the elastic stiffnesses of which there are at most 21 independent values (due to the symmetry of the C matrix with $C_{ij} = C_{ji}$). Christensen (2026) focuses exclusively on wave speeds, but it is important to realize that it is the underlying elastic stiffnesses together with the material density that are more fundamental. The full 21 stiffnesses are required for the least symmetrical triclinic case, but most tectonites will likely not be so complicated and can be described with fewer stiffnesses as illustrated in Figure 2 for isotropic, hexagonal, orthorhombic, monoclinic (for which there are two kinds), and triclinic. The point of this figure is to demonstrate both how the number of elastic constants decreases with increasing symmetry with only 2 for isotropic to the full 21 for triclinic.

As indicated in Christensen (2026), with knowledge of the material's bulk density ρ, the *phase* wave speeds (i.e. those for a hypothetical plane wave) in any direction through the material may be calculated using the Christoffel equation as described in many textbooks (e.g., Auld, 1973) but need not be presented here. Numerous codes are publicly available to make these calculations (Jaeken and Cottenier, 2016; Walker and Wookey, 2012; Yalameha et al., 2022). What solving the Christoffel equation reveals, however, is that for any given direction through the material the solution gives three different wave speeds and their associated particle motions (or polarizations). The three polarizations are orthogonal to one another. That associated with the fastest wave is polarized nearly parallel to the wave propagation direction. The remaining two are polarized nearly transversely to the direction of propagation; the speeds of these two generally differ leading to birefringence commonly referred to as 'shear wave splitting' in the geophysical community.

Often, and as noted in the manuscript, the prefix *'quasi'* is used to describe the wave modes. In an isotropic material the P- and S-wave polarizations are perfectly parallel and perpendicular to the wave propagation direction, respectively. In an anisotropic material, these polarizations deviate from the propagation direction and so the waves are almost but not quite pure P- and S-wave modes. Interestingly, in a hexagonal material one of the S-wave modes is always polarized in the plane perpendicular to the material's axis of symmetry and that is why Christensen (2026) retains for it the term 'S-wave'. The other S-wave mode, however, is not generally polarized with the propagation direction and is hence referred to as a quasi-S wave.

There are two additional related complications that are not generally recognized but ignoring them can lead to difficulties in interpreting seismic observations. First, the Christoffel equation provides *phase*-velocity solutions for plane waves propagating through the material. This can differ significantly from the *group* velocity that is associated with the propagation of energy along a ray from a point source as is what normally is expected in many field seismic observations. Tsvankin (2001) provides a useful review of this topic which is mentioned primarily to warn readers of some of the problems that could be encountered when working with anisotropy between the field and the laboratory. Li et al. (2020) further describes some of the unexpected phenomena associated stemming from this in the context of laboratory measurements. All the results shown in Christensen (2026) are phase velocities.

In special directions the speeds of the two shear wave polarizations will be the same (the shear wave 'kiss' singularity mentioned in Christensen, 2026); this occurs for any direction in an isotropic material and along the line of axial rotational symmetry for hexagonal material. In these cases, the shear wave polarizations lie in the plane perpendicular to the axis of symmetry but are otherwise unconstrained. More usually, however, the polarization of the two shear waves is forced into certain directions dictated by the material properties. For example, of the two 'split' shear waves propagating within the plane perpendicular to the axis of rotation of a hexagonal material, one will be polarized within the plane and the other polarized perpendicular to it.

I am emphasizing this critical point about shear wave polarizations because it must be respected in order to make physically meaningful shear wave velocity measurements. Indeed, Christensen (2026) states that

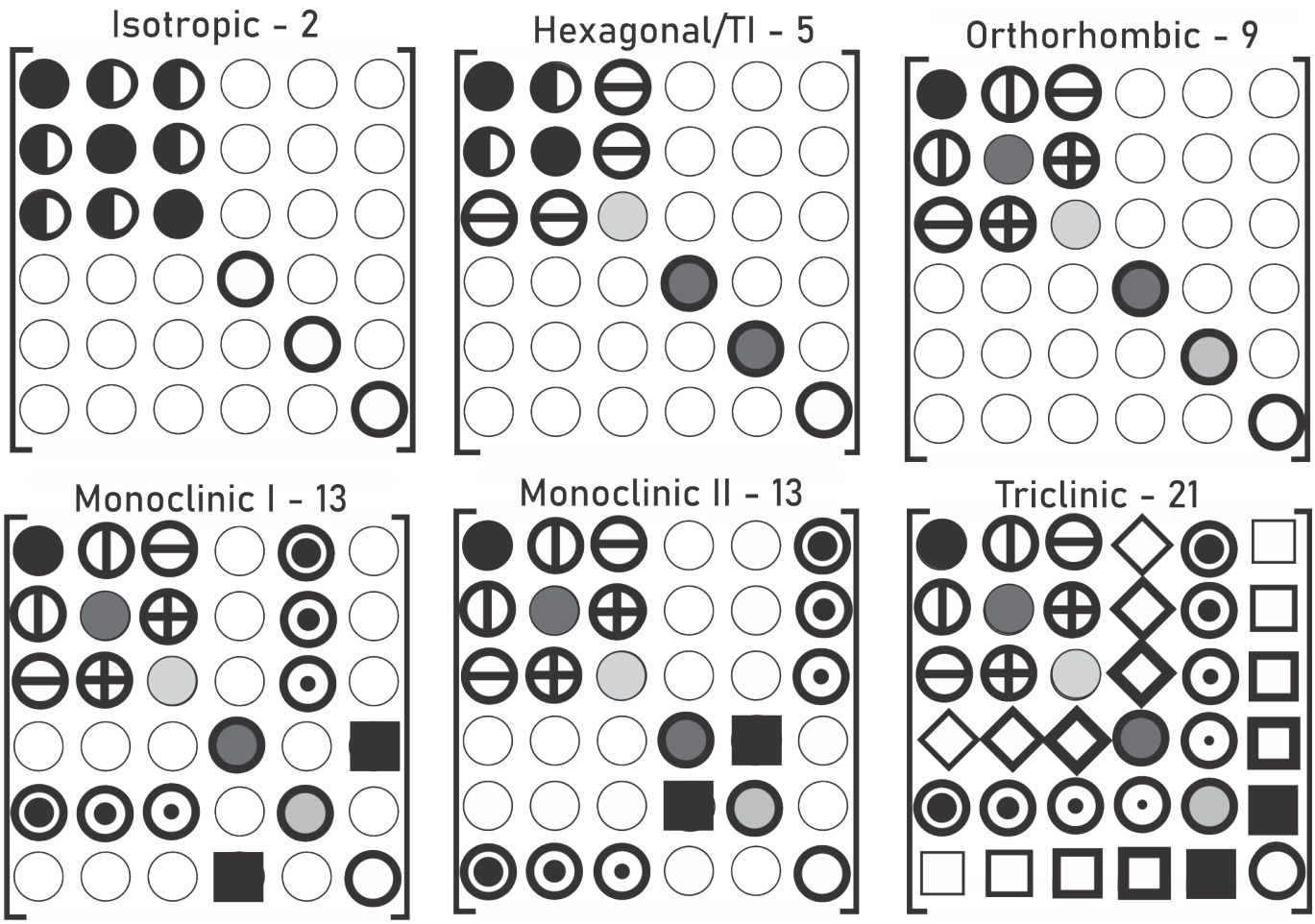

Figure 2 Illustrative Voigt stiffness matrices arranged as shown in Eqn. (1) for the fabric symmetries expected in metamorphic rocks. Empty light circles indicate C_{ij} = 0. Symbols of the same shape indicate equal magnitudes of C_{ij}. Circles with two half shades indicate those dependent stiffnesses calculated from the independent C_{ij} represented by the corresponding solid filled circles. The number of independent stiffnesses required is listed in the title for each symmetry.

'The P-wave and S-wave anisotropies were calculated from velocities measured from 3 orthogonal cores cut from each rock. Two cores were cut with axes parallel to cleavage, foliation, or layering. To obtain information on S-wave splitting in rocks with planar fabrics and/or lineations, two S- velocity pressure runs were made for each core.'

Omitted from this statement is a further key point that he made the two shear wave measurements with the S-wave transducers oriented such that their polarizations are orthogonal to each other and, critically, aligned with the fabric elements. For example, on a sample aligned with the Y-axis in Figure 1b above, one must measure the shear wave speed both with a shear transducer polarized in the X-direction parallel to the foliation and then in the Z-direction perpendicular to the foliation. If this is not done properly then one will still observe a waveform, but it may not be clear how to properly interpret it as over the small sample lengths (a few centimeters) and transit times (~10's of microseconds) the split waves must interfere. Not properly aligning the shear wave polarizations to the rock texture in laboratory measurements is an unrecognized error that appears often in the literature.

3 Converting Velocities to Elastic Moduli

Figures 3 and 8 of Christensen (2026) show several phase velocity surface cross-sections but aside from indicating that they were calculated using the Christoffel equation there were no further details provided. These are calculated using values of the measured elastic stiffnesses C_{ij} that are determined directly from the wave speed measurements, and this aspect needs to be addressed to allow for a full understanding of Christensen (2026). Some of the first applications of ultrasonic wave speed measurements were in the determination of the elastic constants of single crystals (e.g., Huntington, 1947; Neighbours and Schacher, 1967) that prior to these developments were performed using laborious static deformations (see review by Hearmon, 1946). Formulae linking velocities to stiffnesses are complicated, but serendipitously they collapse to simple expressions in certain principal symmetry directions (Auld, 1973; Mah and Schmitt, 2003a,b).

In his Figure 3, the hexagonal case Christensen (2026) provides links to the various wave speed measurements to given directions with simplified expressions. To assist the readers in understanding his Figure 3, is it important to point out that the blue, red, and green cross sections of the wave surfaces correspond to the *qP* mode, the pure S mode polarized within the *XY* plane, and the *qS* mode polarized within the *XZ* plane. One need not consider the *YZ* plane due to the rotational symmetry of the hexagonal case. The observed velocities for the hexagonal symmetry rocks are provided in his Tables 2 and 3 and again some explanation will help readers understand better what was measured and tabulated with *P* being the confining pressure that the rock was subject to in MPa, with the velocities being given in km/s, and with the stiffnesses given in GPa. Also, the angle δ is measured from the rotational axis of symmetry. Finally, from his Figure 3 the linkage between the measured velocities at different angles and the elastic constants are:

Table 2, 3 Designation	Figure 3 Ray	Direct Stiffness
$V_P(0°)$	①	C_{33}
$V_P(90°)_{avg}$	②	C_{11}
$V_P(45°)$	⑤	See Eqn. 2 below for C_{13}
$V_{SH}(90°)$	④	C_{66}
V_{SVavg} (i.e. at 0°)	③	C_{44}

Note that the subscript 'avg' refers to the average of orthogonal measurements arising from the fact that Christensen (2026) made measurements on at least 3 samples in each direction. Examination of the expressions in Figure 3 shows that four of the stiffnesses are determined directly from the observed wave speeds. Note that Tables 2 and 3 do not provide the stiffness C_{66} directly measured using $V_{SH}(90°)$; but instead the value $C_{12} = C_{11} - 2C_{66}$ is reported. Tables 2 and 3 also report values of C_{13}. As indicated in Figure 3, C_{13} is in a multiterm expression but it can be calculated with knowledge of the more easily derived stiffnesses according to (see also Ong et al., 2016)

$$C_{13} = -C_{44} + \sqrt{4\rho^2 V_p^4(45°) - 2\rho V_p^2(45°)(C_{11} + C_{33} + 2C_{44}) + (C_{11} + C_{44})(C_{33} + C_{44})} \tag{2}$$

Propagation of errors through Eqn. 2 severely limit the accuracy of ultrasonically determined measures of C_{13}; this has been one recurring issue in determining the full set of elastic stiffnesses for axial symmetry rocks. More usually this is discussed in the context of the large uncertainty of the Thomsen (1986) anisotropic *'delta'* parameter.

Figure 8 of Christensen (2026) shows a set of 2D profiles of the velocity surfaces for one of the mica schists discussed in the manuscript. Table 4 of the manuscript provides 9 different measured velocities that lie within the three symmetry planes of the orthorhombic rock, and the table below better indicates the linkages between the measured velocities and the illustration of his Figure 8.

Table 4 Velocities	Figure 8 Rays	Direct Stiffnesses
V_{Px}	①	C_{11}
V_{Py}	②	C_{22}
V_{Pz}	③	C_{33}
V_{Pxz}	⑧	See Eqn. 3 below for C_{13}
V_{Pyz}	⑨	See Eqn. 4 below for C_{23}
V_{Pxy}	⑦	See Eqn. 5 below for C_{12}
V_{Szy}	④	C_{44}
V_{Sxz}	⑤	C_{55}
V_{Syx}	⑥	C_{66}

The nomenclature of the wave speeds employed in Christensen (2026) for the orthorhombic case of Table 4 in the manuscript needs some clarification. V_{Px}, V_{Py}, V_{Pz} are the pure P-wave modes that propagate only along the three axes of symmetry of the orthorhombic material, respectively. V_{Pxz}, V_{Pyz}, V_{Pxy} indicate *qP* modes that are propagating within the *XZ*, *YZ*, and *XY* symmetry planes at 45° from either one of the symmetry axes in the plane; and the 45° has been indicated in the equations below for clarity. The designations for the pure shear waves V_{Szy}, V_{Sxz}, and V_{Syx} are not as straightforward to interpret particularly as C_{44}, C_{55}, and C_{66} can be measured in different directions. I expect that the subscripts indicate the symmetry plane within which the given measurement was made.

$$C_{13} = -C_{55} + \sqrt{4\rho^2 V_{pxz}^4(45°) - 2\rho V_{pxz}^2(45°)\,(C_{11} + C_{33} + 2C_{55}) + (C_{11} + C_{55})\,(C_{33} + C_{55})} \tag{3}$$

$$C_{23} = -C_{44} + \sqrt{4\rho^2 V_{pyz}^4(45°) - 2\rho V_{pyz}^2(45°)\left(C_{22} + C_{33} + 2C_{44}\right) + \left(C_{22} + C_{44}\right)\left(C_{33} + C_{44}\right)} \tag{4}$$

$$C_{12} = -C_{66} + \sqrt{4\rho^2 V_{pxy}^4(45°) - 2\rho y(45°)\left(C_{11} + C_{22} + 2C_{66}\right) + \left(C_{11} + C_{66}\right)\left(C_{22} + C_{66}\right)} \tag{5}$$

Similar expressions but cast in terms of different wave speeds are provided by Cheadle et al. (1991) for arbitrary angles of propagation.

4 Wave Phase Velocity Surfaces

The manuscript shows a number of 2-D phase velocity surfaces (Figures 3 and 8), and it is proper to note that these figures borrow from the figure style that Auld (1973) developed to similarly illustrate phase slowness surfaces (i.e., reciprocal of velocity) including the relationships between the elastic stiffnesses and the wave speeds. Christensen (2026) notes that the Christoffel equation may be used to calculate these surfaces. However, it is perhaps also likely that Figures 3 and 8 were created using the simpler (but cumbersome) analytic full expressions that relate phase wave speed to the angle of propagation for axial symmetry (e.g., Thomsen, 1986) or within the three *XY*, *XZ*, and *YZ* symmetry planes for orthorhombic material (e.g., Auld, 1973).

For the sake of completeness, these analytic expressions are worth repeating here as it is likely these equations were used to calculate the wave surfaces in Figures 3 and 8 (Araujo et al., 2018).

The equations for the wave speeds in the 2 different symmetry planes of an axial metamorphic rock (Auld, 1973; Thomsen, 1986) are given below:

4.1 Axial Foliation Plane XY

The *XY* plane in a hexagonal (transversely isotropic) material is also often referred to as the isotropic plane because the three waves speeds to not vary azimuthally. In any direction within the *XY* plane there will be:

- A pure *S* wave mode polarized in the *XY* plane:

$$V_{SXY}^{XY} = \sqrt{\frac{C_{66}}{\rho}} \tag{6}$$

- A second pure *S* wave mode polarized in the *Z* direction:

$$V_{Sz}^{XY} = \sqrt{\frac{C_{44}}{\rho}} = \sqrt{\frac{C_{55}}{\rho}} \tag{7}$$

A pure *P* wave mode polarized in the *XY* plane:

$$V_{Pxy}^{XY} = \sqrt{\frac{C_{11}}{\rho}} = \sqrt{\frac{C_{22}}{\rho}} \tag{8}$$

4.2 Axial Rotationally Symmetric Plane XZ

In the *XZ* plane the phase propagation direction is given by the angle β measured from the *Z*-axis. (perpendicular to the foliation plane). Note that these equations will apply for waves the propagate in any plane that is perpendicular to the foliations *XY* plane.

- Pure *S* wave mode polarized normal to the plane containing the propagation direction

$$V_{Sx}^{XZ} = \sqrt{\frac{C_{44}\cos^2\beta + C_{66}\sin^2\beta}{\rho}} \tag{9}$$

- *qS* wave mode polarized in the *XY* plane:

$$V_{Sxz}^{XZ} = \sqrt{\frac{B_{XZ} - D_{XZ}}{2\rho}} \tag{10}$$

- *qP* wave mode polarized in the *XY* plane:

$$V_{Syz}^{YZ} = \sqrt{\frac{B_{XZ} + D_{XZ}}{2\rho}} \tag{11}$$

where:

$$B_{XZ} = C_{44} + C_{33}\cos^2\beta + C_{11}\sin^2\beta \tag{12}$$

and

$$D_{XZ} = \sqrt{\left[(C_{11} - C_{44})\sin^2\beta + (C_{44} - C_{33})\cos^2\beta\right]^2 + (C_{13} + C_{44})^2\sin^2 2\beta} \tag{13}$$

The equations for wave speeds in the three different symmetry planes of an orthorhombic material are given in Auld (1973). It must be stressed that these equations are valid *only* within the symmetry planes of the material; they should not be used to determine the phase speeds in other directions where the full Christoffel equation solution must be employed.

4.3 Orthorhombic Foliation Plane XY

In the *XY* plane the phase propagation direction is given by angle ϕ measured from the *X*-axis (lineation direction).

- Pure *S* wave mode polarized in the *Z* direction:

$$V_{Sz}^{XY} = \sqrt{\frac{C_{44}\cos^2\varphi + C_{55}\sin^2\varphi}{\rho}} \tag{14}$$

- *qS* wave mode polarized in the *XY* plane:

$$V_{Sxy}^{XY} = \sqrt{\frac{A_{XY} - \sqrt{(A_{XY})^2 - 4C_{XY}}}{2\rho}} \tag{15}$$

- *qP* wave mode polarized in the *XY* plane:

$$V_{Pxy}^{XY} = \sqrt{\frac{A_{XY} + \sqrt{(A_{XY})^2 - 4C_{XY}}}{2\rho}} \tag{16}$$

where:

$$A_{XY} = C_{66} + C_{11}\cos^2\varphi + C_{22}\sin^2\varphi \tag{17}$$

and

$$C_{XY} = \left(C_{11}\cos^2\varphi + C_{66}\sin^2\varphi\right)\left(C_{66}\cos^2\varphi + C_{22}\sin^2\varphi\right) - (C_{12} + C_{66})^2\cos^2\varphi\sin^2\varphi \tag{18}$$

4.4 Orthorhombic Lineation Plane XZ

In the *XZ* plane the phase propagation direction is given by the angle β measured from the *Z*-axis (perpendicular to the foliation plane).

- Pure *S* wave mode polarized in the *Y* direction:

$$V_{Sy}^{XZ} = \sqrt{\frac{C_{66}\cos^2\beta + C_{44}\sin^2\beta}{\rho}} \tag{19}$$

- *qS* wave mode polarized in the *XY* plane:

$$V_{Sxz}^{XY} = \sqrt{\frac{A_{XZ} - \sqrt{(A_{XZ})^2 - 4C_{XZ}}}{2\rho}} \tag{20}$$

- *qP* wave mode polarized in the *XY* plane:

$$V_{Pxz}^{XY} = \sqrt{\frac{A_{XZ} + \sqrt{(A_{XZ})^2 - 4C_{XZ}}}{2\rho}} \tag{21}$$

where:

$$A_{XZ} = C_{55} + C_{33}\cos^2\beta + C_{11}\sin^2\beta \tag{22}$$

and

$$C_{XZ} = \left(C_{55}\cos^2\beta + C_{11}\sin^2\beta\right)\left(C_{33}\cos^2\beta + C_{55}\sin^2\beta\right) - \left(C_{13} + C_{55}\right)^2\cos^2\beta\sin^2\beta \tag{23}$$

4.5 Orthorhombic Orthogonal Plane YZ

In the *XZ* plane the phase propagation direction is also given by the angle β measured from the *Z*-axis (perpendicular to the foliation plane).

- Pure *S* wave mode polarized in the X direction:

$$V_{Sx}^{YZ} = \sqrt{\frac{C_{55}\cos^2\beta + C_{66}\sin^2\beta}{\rho}} \tag{24}$$

- *qS* wave mode polarized in the XY plane:

$$V_{Syz}^{YZ} = \sqrt{\frac{A_{YZ} - \sqrt{(A_{YZ})^2 - 4C_{YZ}}}{2\rho}} \tag{25}$$

- *qP* wave mode polarized in the XY plane:

$$V_{Pyz}^{YZ} = \sqrt{\frac{A_{YZ} + \sqrt{(A_{YZ})^2 - 4C_{YZ}}}{2\rho}} \tag{26}$$

where:

$$A_{XZ} = C_{44} + C_{33}\cos^2\beta + C_{22}\sin^2\beta \tag{27}$$

and

$$C_{XZ} = \left(C_{44}\cos^2\beta + C_{22}\sin^2\beta\right)\left(C_{44}\cos^2\beta + C_{33}\sin^2\beta\right) - \left(C_{23} + C_{44}\right)^2\cos^2\beta\sin^2\beta \tag{28}$$

5 Concluding Comments

I hope that the material above will help readers better appreciate the utility of the Christensen (2026) compilation. Although it is easily obvious by examination that foliated and lineated metamorphic rocks must have orthorhombic symmetry, there still are exceedingly few measurements of the full set of 9 elastic constants for an orthorhombic metamorphic rock and as such the compilation of previously unpublished results is yet another important contribution by Nikolas Christensen.

References

Araujo, E., Alcalde, R., and Balazs, N. Constraining in Situ Stresses in Southern Saskatchewan, Canada. In *52nd U.S. Rock Mechanics/Geomechanics Symposium*, 2018.

Auld, B. *Acoustic fields in waves and solids*, volume 1. John Wiley and Sons, 1973.

Brugger, K. Pure Modes for Elastic Waves in Crystals. *Journal of Applied Physics*, 36(3):759–768, Mar. 1965. doi: 10.1063/1.1714215.

Cheadle, S. P., Brown, R. J., and Lawton, D. C. Orthorhombic anisotropy; a physical seismic modeling study. *Geophysics*, 56(10):1603–1613, Oct. 1991. doi: 10.1190/1.1442971.

Cholach, P. Y., Molyneux, J. B., and Schmitt, D. R. Flin Flon Belt seismic anisotropy: elastic symmetry, heterogeneity, and shear-wave splitting. *Canadian Journal of Earth Sciences*, 42(4):533–554, Apr. 2005. doi: 10.1139/e04-094.

Christensen, N. I. A compilation of elastic anisotropy measurements from metamorphic rocks. *Seismica*, 5, 2026. doi: 10.26443/seismica.v5i1.1570.

Crampin, S. An introduction to wave propagation in anisotropic media. *Geophysical Journal International*, 76(1):17–28, Jan. 1984. doi: 10.1111/j.1365-246x.1984.tb05018.x.

Hearmon, R. F. S. The Elastic Constants of Anisotropic Materials. *Reviews of Modern Physics*, 18(3):409–440, July 1946. doi: 10.1103/revmodphys.18.409.

Huntington, H. B. Ultrasonic Measurements on Single Crystals. *Physical Review*, 72(4):321–331, Aug. 1947. doi: 10.1103/physrev.72.321.

Jaeken, J. W. and Cottenier, S. Solving the Christoffel equation: Phase and group velocities. *Computer Physics Communications*, 207:445–451, Oct. 2016. doi: 10.1016/j.cpc.2016.06.014.

Klein, C., Hurlbut, C., and Dana, J. Manual of Mineralogy (after James D. Dana). Wiley., 1993. https://books.google.com/books?id=8ybwAAAAMAAJ.

Li, W., Schmitt, D. R., and Chen, X. Accounting for pressure-dependent ultrasonic beam skew in transversely isotropic rocks: combining modelling and measurement of anisotropic wave speeds. *Geophysical Journal International*, 221(1):231–250, Jan. 2020. doi: 10.1093/gji/ggz580.

Mah, M. and Schmitt, D. R. Correction to "Determination of the complete elastic stiffnesses from ultrasonic phase velocity measurements". *Journal of Geophysical Research: Solid Earth*, 108(B10), Oct. 2003a. doi: 10.1029/2003jb002710.

Mah, M. and Schmitt, D. R. Determination of the complete elastic stiffnesses from ultrasonic phase velocity measurements. *Journal of Geophysical Research: Solid Earth*, 108(B1), Jan. 2003b. doi: 10.1029/2001jb001586.

Neighbours, J. R. and Schacher, G. E. Determination of Elastic Constants from Sound-Velocity Measurements in Crystals of General Symmetry. *Journal of Applied Physics*, 38(13):5366–5375, Dec. 1967. doi: 10.1063/1.1709328.

Nye, J. *Physical properties of crystals; their representation by tensors and matrices*. Clarendon press, 1985.

Ong, O. N., Schmitt, D. R., Kofman, R. S., and Haug, K. Static and dynamic pressure sensitivity anisotropy of a calcareous shale. *Geophysical Prospecting*, 64(4):875–897, June 2016. doi: 10.1111/1365-2478.12403.

Paterson, M. S. and Weiss, L. E. Symmetry Concepts in the Structural Analysis of Deformed Rocks. *Geological Society of America Bulletin*, 72(6):841, 1961. doi: 10.1130/0016-7606(1961)72[841:scitsa]2.0.co;2.

Thomsen, L. Weak elastic anisotropy. *Geophysics*, 51(10):1954–1966, Oct. 1986. doi: 10.1190/1.1442051.

Tsvankin, I. *Seismic signatures and analysis of reflection data in anisotropic media*. Society of Exploration Geophysicists, Jan. 2001. doi: 10.1190/1.9781560803003.

Walker, A. M. and Wookey, J. MSAT—A new toolkit for the analysis of elastic and seismic anisotropy. *Computers & Geosciences*, 49:81–90, Dec. 2012. doi: 10.1016/j.cageo.2012.05.031.

Winterstein, D. F. Velocity anisotropy terminology for geophysicsts. *Geophysics*, 55(8):1070–1088, Aug. 1990. doi: 10.1190/1.1442919.

Yalameha, S., Nourbakhsh, Z., and Vashaee, D. ElTools: A tool for analyzing anisotropic elastic properties of the 2D and 3D materials. *Computer Physics Communications*, 271:108195, Feb. 2022. doi: 10.1016/j.cpc.2021.108195.